Journal of Applied Polymer Science

Alignment and Properties of Carbon Nanotube Buckypaper/Liquid Crystalline Polymer Composites

Chi-Yung Chang,[1,2] Erin M. Phillips,[2] Richard Liang,[2] Stanley W. Tozer,[3] Ben Wang,[2] Chuck Zhang,[2] Hsien-Tang Chiu[1]

[1]Department of Material Science and Engineering, National Taiwan University of Science and Technology, Taipei 106, Taiwan
[2]High-Performance Materials Institute and Department of Industrial and Manufacturing Engineering, Florida State University, Tallahassee, Florida 32310
[3]National High Magnetic Field Laboratory, Tallahassee, Florida 32310
Correspondence to: C.-Y. Chang (E-mail: D9604010@mail.ntust.edu.tw)

ABSTRACT: Carbon nanotubes (CNTs) have been recognized as a potential superior reinforcement for high-performance, multifunctional composites. However, non-uniform CNT dispersion within the polymer matrix, the lack of adequate adhesion between the constituents of the composites, and lack of nanotube alignment have hindered significant improvements in composite performance. In this study, we present the development of a layer-by-layer assembly method to produce high mechanical performance and electrical conductivity CNT-reinforced liquid crystalline polymer (LCP) composites using CNT sheets or buckypaper (BP) and self-reinforcing polyphenylene resin, Parmax. The Parmax/BP composite morphology, X-ray diffraction, mechanical, thermal, and electrical properties have been investigated. SEM observations and X-ray diffraction demonstrate alignment of the CNTs due to flow-induced orientational ordering of LCP chains. The tensile strength and Young's modulus of the Parmax/BP nanocomposites with 6.23 wt % multi-walled carbon nanotube content were 390 MPa and 33 GPa, respectively, which were substantially improved when compared to the neat LCP. Noticeable improvements in the thermal stability and glass transition temperature with increasing CNT content due to the restriction in chain mobility imposed by the CNTs was demonstrated. Moreover, the electrical conductivity of the composites increased sharply to 100.23 S/cm (from approximately 10^{-13} S/cm) with the addition of CNT BP. These results suggest that the developed approach would be an effective method to fabricate high-performance, multifunctional CNT/LCP nanocomposites. © 2012 Wiley Periodicals, Inc. J. Appl. Polym. Sci. 000: 000–000, 2012

KEYWORDS: nanocomposites; liquid crystals; nanotubes; graphene and fullerenes; structure–property relations

Received 28 January 2012; accepted 16 June 2012; published online
DOI: 10.1002/app.38209

INTRODUCTION

Carbon nanotubes (CNTs) have attracted tremendous attention due to their unique combination of electronic, mechanical, chemical, and thermal properties,[1–3] which has built upon Iijima's pioneering research reported in 1991.[4] CNT sheets, or buckypaper (BP), are free-standing mats of entangled carbon nanotube ropes.[5] BP can be readily fabricated into sizable products through a CNT suspension and filtration process and should prove to be convenient for use in various composite fabrication methods. The electrical conductivity,[6] field emission properties,[7] gas permeability,[8] electronic properties, and mechanical properties of BP have undergone extensive studies.[9] Numerous research efforts have been carried out to explore the potential applications of BP, including CNT actuators,[10] artificial muscles,[11] strain sensors,[12] and cold field emission cathodes.[7] CNTs and CNT BP can be used to improve the mechanical and physical property of polymers for functional and structural applications.[13–15] The mechanical and physical property of CNT composites strongly depend on the homogeneous dispersion of CNTs in the polymer matrix, as well as good interfacial adhesion between CNTs and the polymer matrix. However, dispersion of CNTs into the polymer matrix is extremely difficult due to van der Waals interactions between the nanotubes leading to their tendency to agglomerate during composites fabrication processes.[16] Particularly, uniformly dispersing CNTs in high viscosity thermoplastic resins without the use of solvents and strong sonication aids is challenging.[17] The use of BP is an effective way to avoid nanotube agglomeration and help compensate for processing difficulties due to high polymer viscosity, to achieve uniform dispersion and high CNT concentration

within the polymer matrix.[15] What is more, much effort has been invested in recent years to align the CNTs. Commonly used approaches including magnetic and electric fields, shear flow, and mechanical ordering as well as aligned growth have been investigated,[18–22] most of which are dependent on the application of external fields.

Liquid crystalline polymers (LCPs) are very attractive for composite applications due to their exceptional mechanical properties and unique microstructures, compared to conventional thermoplastic polymers.[23] The orientational ordering of LCP chains in the melt phase distinguishes them from the isotropic melt phase of conventional engineering thermoplastics at high temperatures.[23,24] The ordering of the liquid crystalline phase is a molecular scale phenomena and this ordering can be either temperature or concentration dependent.[23,24] Thermotropic LCPs show two distinct phases: nematic and smectic. In the nematic phase, molecules have no positional order, but they point in the same direction. In the smectic phase, the molecules tend to align themselves in layers and planes.

The alignment of LCP molecules is crucial to its mechanical and electrical properties.[25,26] LCP alignment can be achieved through several processes. For example, it has been reported that for a dip-coated LCP polymer film, the molecules tend to align in the direction of withdrawal from the polymer solution.[25,26] Buffing is another process that has proven to facilitate LCP molecular alignment. During buffing, polymer chains in smectic and nematic phases can be homogeneously aligned in the direction of the shear force in the solid state, and the alignment is believed to be caused by the application of shear force on the LCP film.[24–26] During the processes, the polymer seems to become trapped between a moving and a stationary phase. The movable source exerts a shear force on the polymer molecules, causing them to align in the direction of the shear force.[25,26]

This technique has been frequently used for aligning such nanoscale inclusions along the flow direction to increase the mechanical properties. Interesting interactions of LCP orientation and CNTs have been reported; Song et al. first demonstrated the nematic liquid crystallinity of MWNTs in water.[27] Examination of a series of aqueous dispersions with different MWNT concentrations showed a phase transition from isotropic to a Schlieren texture typical of lytropic nematic liquid crystals above a critical concentration of $\sim$ 4.3% by volume. Similarly, Lynch and Patrick oriented the nematic low molar mass LCP in an electric field and used these matrices to align the suspended MWNTs.[28] The MWNTs were oriented along the direction of applied electric field, and a 1.8 V/μm electric field was strong enough to overcome the orientational effect of the grooves, which were perpendicular to the electric field. Later, Mrozek et al. reported that the ordered SWNTs could be used to organize the LCP via kinetic seeding of homogeneous liquid crystal domains from an LCP melt.[29]

Other major challenges for the fabrication of CNT-reinforced polymer composites are optimizing the processing steps and reducing the manufacturing cost. Among various processing techniques mentioned above, hot press molding coupled with layer-by-layer assembly method has shown great potential toward fabricating high performance polymer composites for industrial applications at lower processing costs, which can facilitate commercial scale-up.[26]

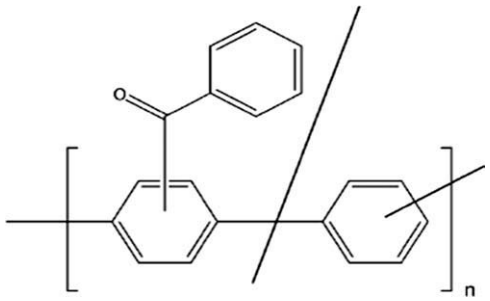

Figure 1. Parmax liquid crystalline polymer (LCP) molecular structure.

In this study, we demonstrate the integration of well dispersed CNT BP in LCP matrix for the first time. Moreover, our approach is different from the previous reported works mentioned above because the CNT networks are first employed and then incorporated in the preformed LCP matrix as fillers. In the earlier works, only the nanotubes themselves form LCP ordering. The LCP/BP composites were produced using a combination of hot press molding and simple lay-up assembly of LCP and BP layers. The effectiveness of fabrication process, mechanical, thermal, and electrical properties of the resultant samples are studied and analyzed.

EXPERIMENTAL

Materials

Multi-walled carbon nanotubes (MWNTs) purchased from Nanocomp Technologies Inc. (Concord, NH) consist of millimeter-long, high purity (>90 wt %) and small-diameter ($\sim$ 3–8 nm) MWNTs with a range of 2–5 walls, providing a aspect ratio up to 1000.[30]

The LCP used was poly[(benzoyl-1,4-phenylene)-*co*-(1,3-phenylene)] trademarked as Parmax®, batch number as 1200 and was obtained from Mississippi Polymer Technologies Inc. Parmax is a copolymer of *para*-linked benzophenone and *meta*-linked unsubstituted phenylene units,[24] as shown in Figure 1. These copolymers are commonly referred to as self-reinforced polymers (SRPs) because of their intrinsic high strength and modulus without addition of a reinforcing agent. Parmax has high mechanical strength and stiffness, and outstanding thermal stability. The tensile strength of neat Parmax is $\sim$ 207 MPa, rockwell hardness (80 B), tensile modulus (5.5 GPa), and molecular weight (26,900–30,000).[31] All materials were used as received without further purification or treatment.

Preparation of MWNT Buckypaper

The MWNTs were first made into BPs, which are thin films of preformed nanotube networks.[32] Aqueous suspensions were prepared by mixing the MWNTs with suitable surfactant and distilled water under ultrasonic power 85 W/m^2 for about 60 min.[33,34] These nanotube suspensions, which can remain stable for more than two months, were pumped through a nylon filter membrane. After filtration, the MWNT BP was peeled from the

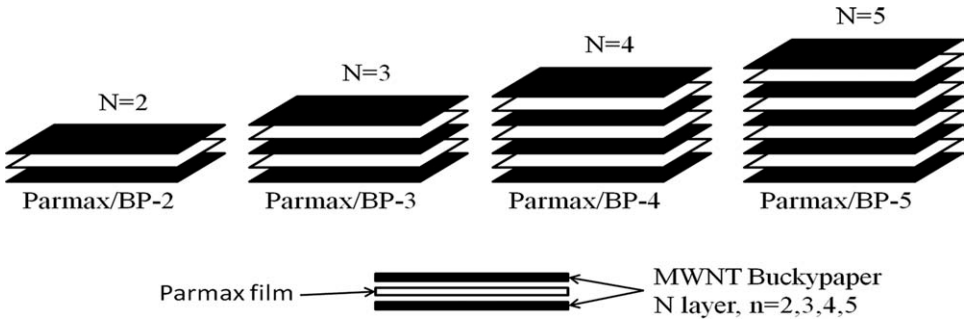

Figure 2. Schematic diagram of preparation of laminate structure Parmax/BP composites.

filter membrane. Finally, the BP was thoroughly washed with isopropanol to remove the adsorbed surfactant, resulting in a thin membrane with 10–25 μm thickness.

Composite Preparation

Firstly, the as-received Parmax pellets were hot pressed in a 10 ton hydraulic Carver press (Wabash, IN), a 5 cm × 5 cm Teflon plate mold was used to produce the Parmax films and the thickness of Parmax film was approximately of 0.5 mm. Secondly, the MWNT BP and Parmax films were carefully laid up in various laminate configurations, respectively as shown in Figure 2. For example, the sample Parmax/BP-2 comprised BP/Parmax/BP sandwich structure via layer-by-layer assembly.[35] Finally, the different Parmax/BP laminates were held tightly by pressing of ~ 2000 psi at 270°C for 30 min under a 5 cm × 5 cm Teflon plate mold, respectively, which was then allowed to cool to room temperature. The composite films with different Parmax/BP laminates and 0.5–2.3 mm thick were obtained using layer-by-layer assembly method. The layer-by-layer assembly method allowed the flexibilities to control the contents of CNTs in the composite film, the overall thickness, and the distance between the individual nanotubes.[36] In this study, no distinct interfaces between layers were observed due to full infiltration of LCP into BP under pressing. The weight fraction of MWNTs in each composite film was calculated using the weight of the BP divided by the total mass of the final composite samples, as shown in Table I.

Characterization

Scanning Electron Microscopy. Scanning electron microscopy (SEM) measurements were performed with a field emission scanning electron microscope (JEOL 7401F) using a voltage of 10 kV. The cross-sections were attained by brittle fracture of the composite in the direction parallel to the shear flowing direction in liquid nitrogen, and then the samples were sputter coated with an Au–Pd alloy, at a covering time of 120 s at 20 mÅ.

Table I. Parmax/Buckypaper (BP) Composite Sample Parameters

Sample name	MWNT BP layers	Thickness (mm)	MWNT content (wt %)
Parmax/BP-2	2	0.55	1.13 ± 0.15
Parmax/BP-3	3	1.32	2.57 ± 0.24
Parmax/BP-4	4	1.63	4.62 ± 0.45
Parmax/BP-5	5	2.24	6.23 ± 0.30

X-Ray Diffraction. Wide- and small-angle X-ray diffractograms (SAXS, WAXD) were obtained using a Brucker Nanostar diffractometer with an IμS microfocus X-ray source, which was equipped with a Histar 2D Multiwires SAXS detector and a Fuji Photo Film FLA-7000 scanner at ambient temperature. SAXS profiles were calibrated with silver behenate and WAXD patterns with corundum. Both standards were obtained from Brucker.

A characteristic feature of X-ray patterns from a uniaxial oriented sample is the presence of arcs. The azimuthal width of the arcs provides information about the degree of the orientation of the respective scattering planes. The relative intensity along the azimuthal, $(I(\psi))$, at 2Θ is related to the orientation distribution function (ODF) of the scattering planes. Approximating the ODF as a Legendre polynomial series in cos ψ, the Herman's orientation parameter S_d (sometimes referred to as P_2) is the second moment average of the ODF and expressed as:

$$s_d = \frac{3(\cos^2 \varphi) - 1}{2} \quad (1)$$

For uniaxial orientation, S_d assumes values from −0.5 to 1. A value of −0.5 reflects perfect alignment in the plane perpendicular to the uniaxial direction; 0 reflects random orientation; and 1 reflects alignment along the uniaxial direction.[37]

Thermogravimetric Analysis. The thermal stability of the composites was analyzed using thermogravimetric analysis (TGA). The measurements were carried out with a TA Instruments TA-Q50 at a heating rate of 10 °C/min under a nitrogen atmosphere. The analysis was performed on samples with an average mass of 10 mg from room temperature to 800°C.

Differential Scanning Calorimetry. The phase transition behavior of the composites was investigated using differential scanning calorimetry (DSC) under nitrogen flow. The DSC used was TA Instruments TA-Q100. Samples of approximately 10 mg were weighed and sealed in standard aluminum sample pans. Prior to the heating and cooling scans, the composites were melted at 300°C and maintained at this temperature for 5 min in order to eliminate the thermal history of the material. They were then cooled from 300°C to 40°C at a rate of 10 °C/min,

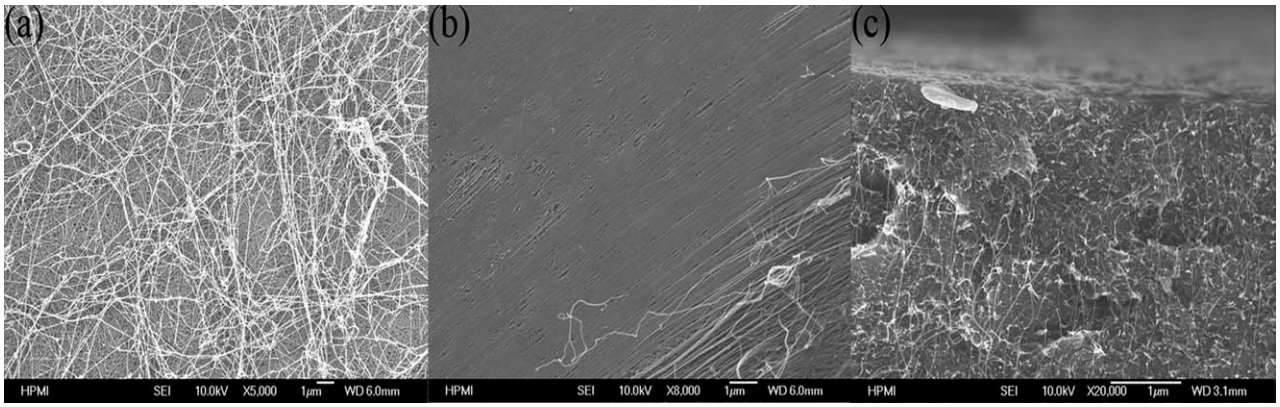

Figure 3. SEM images of (a) CNT BP displaying uniform dispersion, (b) surface morphology of a 5 layer LCP/BP composite sample (Parmax/BP-5), (c) cross-sectional morphology of a 5 layer LCP/BP composite sample (Parmax/BP-5).

and then heated from 40°C to 300°C at 10 °C/min to conduct the measurements.

Dynamic Mechanical Analysis. The mechanical performance of the composites was studied using dynamic mechanical analysis (DMA) on a TA Instruments DMA Q-800. Rectangular shaped samples of 19.5 mm long, 4 mm wide, and thicknesses as detailed in Table I were mounted in a large tension clamp. Measurements were performed at a fixed frequency of 1 Hz in the tensile mode. For each sample, the temperature was ramped from 50°C to 250°C, at a 2 °C/min heating rate.

Tensile Properties. Tensile properties of the composite samples were measured using a Shimatsu AGS-J materials testing system (Kyoto, Japan) at room temperature (23 ± 2)°C, (40 ± 5)% relative humidity, with a crosshead speed of 1 mm/min on a 500 N load cell. Dog-bone shaped specimens (Type V) as specified in the ASTM standard D638 were cut parallel to the polymer shear flowing direction. The samples were conditioned for 24 h prior to obtaining the experimental measurements, and at least three specimens of each composite type were tested to ensure reproducibility.

Electrical Conductivity. Electrical conductivity was measured with Keithley 2000 (Cleveland, OH) multimeters and a DC voltage/current source using the four-probe method through the computer controlled LabVIEW program. A typical DC bias voltage of 20 mV to 1 V was applied across the composite films, and the output current was monitored and recorded. The corresponding electrical conductivity (σ) was calculated and expressed as:

$$\sigma = \frac{1}{\rho_b} = \frac{L}{R \times W \times t} \quad (2)$$

Here σ is the measured conductivity and ρ_b, L, W, and t are the bulk resistivity, length, width, and thickness of the sample, respectively.

RESULTS AND DISCUSSION

Microstructure Analysis

The surface and cross-sectional morphologies of the composite samples were investigated using SEM. Uniform CNT dispersion and good adhesion between the CNTs and the Parmax matrix can be seen in Figure 3. The surface morphology of the MWNT BP without any treatment was also seen in Figure 3(a). From Figure 3, the CNTs appear to be homogeneously dispersed without aggregation in the Parmax matrix. The CNTs also appear to exhibit orientational alignment most likely due to strong interactions with LCP chains during the fabrication process.[38] Parmax molecular chain is highly aromatic, and this high degree of aromaticity attributes to the high chain stiffness. Moreover, the strong "π-stacking" between CNT and Parmax coupled with the Parmax smectic morphology helps to disperse and align CNTs during the flow stage of processing.[38] Therefore, the aromatic ring structure of Parmax is able to strongly interact with the nanotube surface through intermolecular overlap π-stacking.

Moreover, in the melt during the process, the LCP molecules tend to align themselves along the flow direction, and there is a shear contribution in the flow. Simultaneously, the randomly distributed BP layers are well aligned along the shearing direction induced by the LCP molecules and well-oriented LCP/BP composite films are formed by a simple hot pressing.[38,39] The CNT alignment among the LCP matrix can be observed clearly in Figure 3(b,c). Good wetting and adhesion of the CNTs with the LCP were also apparent, indicating a strong interaction and compatibility between the CNTs and the polymer matrix.

X-Ray Diffraction Analysis

Figure 4 shows the integrated X-ray diffraction intensity of pure Parmax and Parmax/BP composites, where the peak maximum correlates to the average lateral spacing between polymer chains. As seen in Figure 4, the wide peak of Parmax at 19.93° was observed,[40] and the corresponding 0.445 nm d-spacing was calculated. While introducing BP into Parmax, it can be seen that the relative intensities of MWNT diffraction peaks increase with increasing MWNT concentration. Thus, the Parmax/BP-5 composites sample showed a strong diffraction of the (002) crystal planes of MWNTs, as shown in Figure 4,[41] with a 0.336 nm calculated d-spacing. When the nanotubes have preferred orientation, the Bragg intensities will be concentrated at two spots at the intersections of the plane defined by K_i (incident X-ray beam) and Q_{002} (reciprocal space vector), and the powder ring, as shown in Figure 5.[41] Figure 6 depicts a 2D WAXD pattern

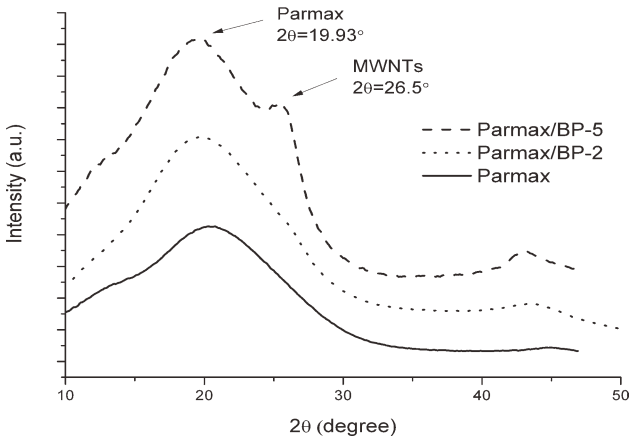

Figure 4. Integrated X-ray diffraction intensity of neat Parmax, Parmax/BP-2 nanocomposite (1.13 wt % MWNT), and Parmax/BP-5 nanocomposite (6.23 wt % MWNT).

for Parmax/BP-5 composite where two pairs of intense Bragg arcs can be observed. These two pairs of diffractions can be assigned as the Parmax and MWNT, respectively. From Figure 6, the location of the Bragg arcs with respect to the incident beam indicated the longitudinal axes of the nanotubes are parallel to the molecular chain direction of the polymer.[42]

To confirm this indication, the 2D WAXD intensity data were integrated along the 2Θ axis and plotted as I versus azimuth ψ after subtracting out the background intensity, as shown in Figure 7. Figure 7 shows two distinct peaks, which were found to be centered at $\psi = 0°$ and 180°. The fitted full width at half maximum of Parmax/BP-5 nanocomposite was 55° and the Herman's orientation factor described above was calculated to be 0.72. This suggests that the confined nanotubes were aligned parallel to the molecular chains of the Parmax during the hot press processing. A shearing force may be generated during hot pressing, causing the induced orientation for both the CNTs and Parmax chains as illustrated in Figure 8, which enhances the stress transfer between the polymer and the nanotubes, thus leading to the improvements in the strength and Young's modulus.[38]

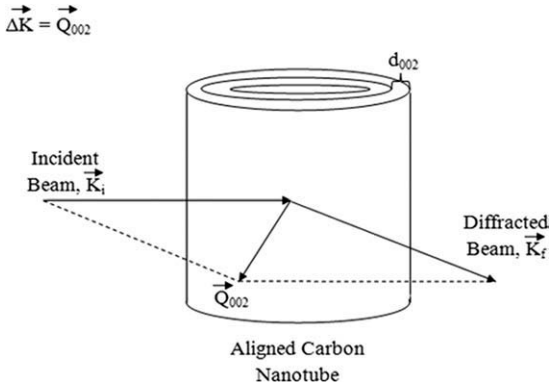

Figure 5. Schematic of X-ray diffraction of a MWNT demonstrating Bragg's law. Perpendicular to the longitudinal axis of the MWNT, the incident beam (K_i), diffracted beam (K_f), and reciprocal space vector (Q_{002}) lie on the same plane.

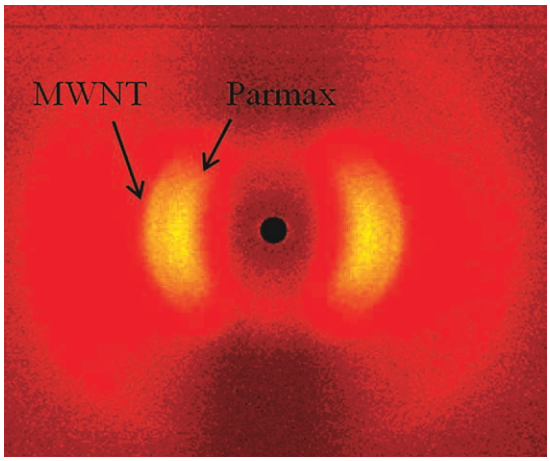

Figure 6. 2D WAXD pattern image of the Parmax/BP-5 nanocomposite (6.23 wt % MWNT). [Color figure can be viewed in the online issue, which is available at wileyonlinelibrary.com.]

Thermal Stability

Figure 9 displays and compares the effects of increased concentration of MWNTs on the thermal stability of the composites to the neat Parmax sample. The decomposition under an inert environment (nitrogen) takes place in a single stage for all samples. This single stage decomposition process may involve decarboxylation, decarbonylation, and dehydration.[43] The aromatic structure remains as the residue goes up to very high temperature.[44] The weight loss of the Parmax/BP composites at high temperatures is primarily attributed to the breakdown of the polymer chains. Figure 9 indicates the neat Parmax begins to degrade at approximately 486°C. The degradation temperature (T_d) consistently increases with increasing MWNT concentration (Parmax/BP-2 : 503°C, Parmax/BP-3 : 524°C, Parmax/BP-4 : 558°C). The T_d of the Parmax/BP-5 sample (6.23 wt % MWNT) displayed a T_d of 583°C, an approximate 100°C increase compared with the neat Parmax control sample. The increase in T_d with increasing MWNT concentration indicates improved thermal stability of the composites compared with the neat Parmax. At 800°C, Parmax has residual weight around 1.23% and Parmax/BP-2 shows

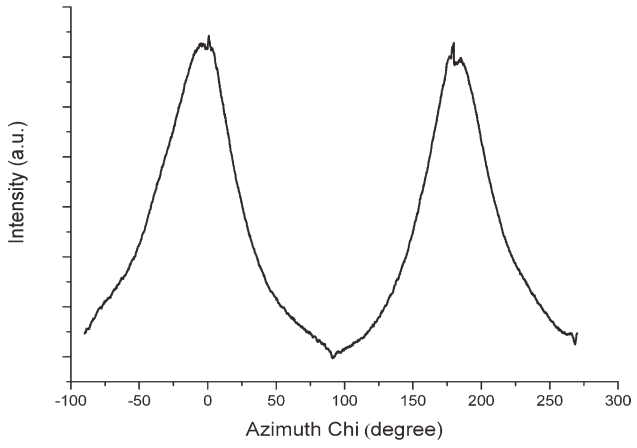

Figure 7. Integrated 2D WAXD intensity displaying the azimuth peaks for nanotubes in the Parmax/BP-5 nanocomposite (6.23 wt % MWNT).

Applied Polymer SCIENCE

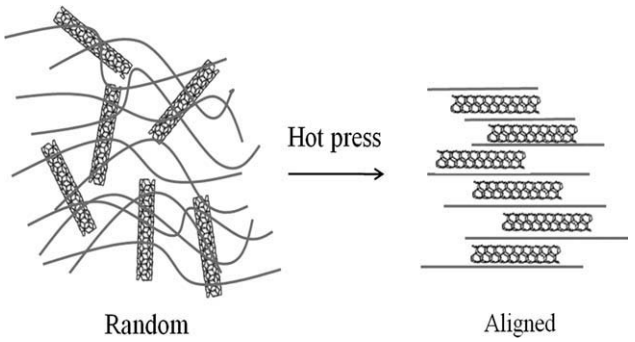

Figure 8. Schematics of nanotubes parallel to the molecular chain direction of the polymer after hot press processing.

residual weight of 2.54%, which increased after the introduction of MWNTs into LCP. The Parmax/BP-3 shows a residual weight of around 4.46%, which further increased to 5.61% for Parmax/BP-4 and 8.06% for Parmax/BP-5. This finding suggests that MWNTs have a positive influence on the thermal stability of LCP.

The presence of polymer chains near the nanotube molecular surface may hinder polymer degradation due to molecular interactions, which may noticeably decrease molecular chain mobility,[45] and thus result in the increased shift of the T_d of the composite samples to higher temperature. Another explanation for the increased thermal stability of the polymer composites may be credited to the effects of increased thermal conductivity with increasing MWNT concentration.[46] This increased conductivity, due to the presence of thermally conductive nanotubes, facilitates heat dissipation within the composite and therefore increases the overall thermal stability.[46] From the experimental results, it can be proved that Parmax nanocomposites reinforced with small quantity of MWNTs performed better in regards to thermal stability and lower degradation rate compared with neat Parmax.

Phase Transition Behavior

DSC was used to evaluate the effects of MWNTs on the phase transition behavior of the Parmax/BP composites, as shown in

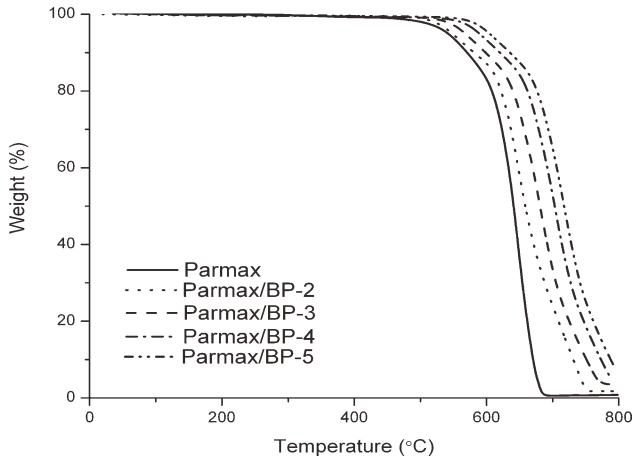

Figure 9. TGA degradation trend of Parmax/BP composite samples compared to neat Parmax indicating the effect of MWNT concentration on the degradation temperature.

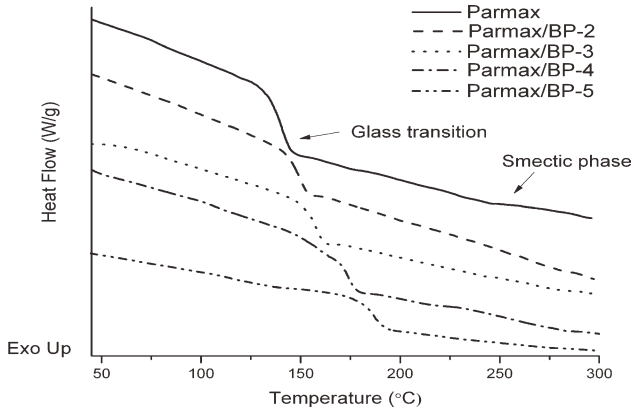

Figure 10. DSC trends showing the effect of MWNTs on the phase transition behavior of the Parmax/BP composites compared to the neat Parmax.

Figure 10. The neat Parmax sample had a glass transition temperature of approximately 155°C and a smectic phase melting transition of approximately 270°C.[47] In the smectic phase, the MWNTs tended to align in the orientation of the polymer chains due to the LCP molecule chain alignment, thus the processing temperature for composite fabrication during the hot press molding was conducted at 270°C corresponding to the smectic phase of the polymer.

The glass transition temperature (T_g) of each Parmax/BP composite sample was determined using DSC. The T_g was observed to increase with the increasing MWNT concentration, as shown in Figure 10. For example, Parmax/BP-5 (6.23 wt % MWNT) had a T_g of approximately 190°C, while the neat Parmax had a T_g of approximately 155°C. This increase correlated to the presence of molecular interactions between the Parmax LCP and the MWNTs of the BP. The nanotubes may be restricting the polymer chain mobility, causing an increase in the T_g. This effect can also be understood in terms of decreasing free volume of the polymer due to possible strong "π-stacking" interactions.[45]

The steady increase in T_g with nanotube concentration may also be due to the formation of a secondary CNT network structure in addition to the primary entanglement of the polymers, causing immobilization of the polymer chains at elevated temperatures.[48] In addition, the presence of MWNT agglomerations in polymer composites has been reported to lead to a decrease in the T_g[49]; therefore, the increase in the T_g with relatively high nanotube concentration, as seen in this work, may suggest the absence of significant agglomerations.

Dynamic Mechanical Properties

In terms of mechanical performance, the storage modulus of a polymer can be used to describe its stiffness. The storage modulus of the composite samples dramatically increased with the incorporation of a relatively small amount (1.13 wt % MWNT) of MWNTs in the Parmax matrix, as shown in Figure 11. Over most of the temperature range tested, the storage modulus increased with increasing nanotube concentration. This indicates that the presence of MWNTs enables the polymer matrix to sustain its stiffness at a higher temperature range (near the T_g).[47]

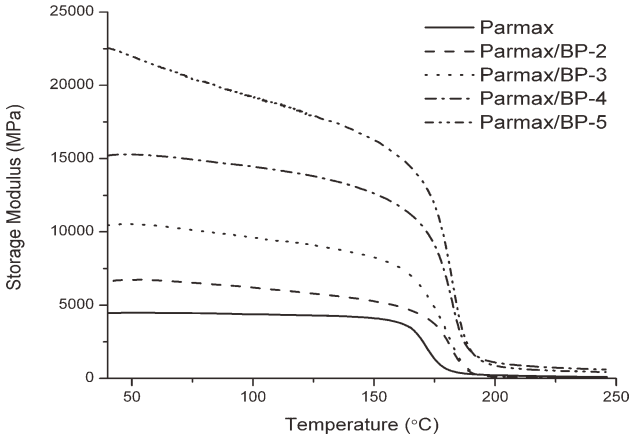

Figure 11. DMA trends showing the effect of MWNT concentration of the composite samples on the storage modulus, compared to neat Parmax.

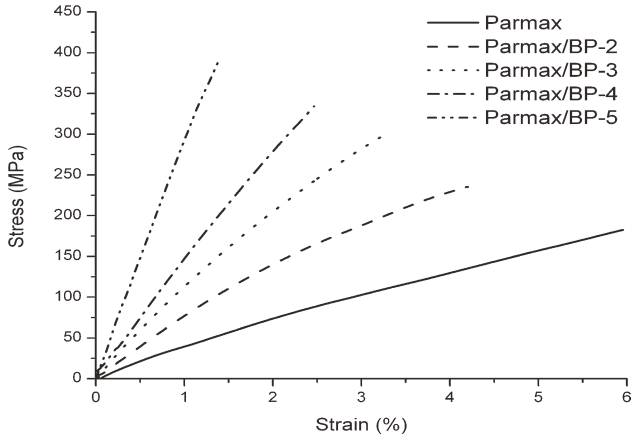

Figure 12. The effect of MWNT concentration on the stress–strain curves of Parmax/BP nanocomposites compared to neat Parmax.

The Parmax/BP-5 composite sample (6.23 wt % MWNT), for example, showed an increase in storage modulus of approximately 400% (21,800 MPa) at room temperature compared to the neat Parmax sample (4463 MPa). This increased storage modulus is attributed to the effect of the homogeneous dispersion of MWNTs in the LCP matrix coupled with significant nanotube/polymer interactions, resulting in the enhanced adhesion between the MWNTs and the matrix. The storage modulus of polymer matrix composites was also shown to be strongly dependent on polymer microstructure and crystallinity. By coupling the DMA results with the DSC results, it can be concluded that the increase in the storage modulus of the composite samples was also influenced by the polymer matrix crystallinity.[38] In addition, From X-ray diffraction results, the Parmax/BP-5 composite showed the higher diffraction intensity compared to neat Parmax. Thus, for the Parmax/BP-5 composite, the percent crystallinity became higher with increasing MWCNT concentration. It indicates that MWNTs promoted the crystallization of Parmax LCP, which was more prominent in the enhancement of storage modulus in Parmax/BP-5 composite with 6.23 wt % MWNTs.[38]

Tensile Properties

Table II and Figure 12 show the effects of MWNT BP on the mechanical properties of the composites. Figure 11 shows that the presence of MWNTs improved the tensile properties compared to the neat Parmax sample. The Young's modulus and tensile strength for the neat Parmax were approximately 3.92 GPa and 182 MPa, respectively, which are in agreement with the manufacturer datasheet.[30] As the MWNT concentration increased, the Young's modulus and tensile strength of Parmax/BP-5 both significantly increased, up to a 750% (33 GPa) and a 110% (390 MPa), respectively, compared to those of the neat Parmax sample. However, the elongation at break, which is a direct indicator of a material's toughness, decreased sharply with the increasing MWNT content which is also due to an increased restriction of LCP molecular chain mobility.

Table II. Mechanical Properties of Parmax/Buckypaper (BP) Composite Samples

Sample name	Young's modulus (GPa)	Tensile strength (MPa)	Elongation at break (%)
Neat Parmax	3.92 ± 1.02	182.5 ± 9.54	5.95 ± 1.32
Parmax/BP-2	6.20 ± 2.11	235.4 ± 5.43	4.20 ± 1.03
Parmax/BP-3	9.93 ± 1.49	298.9 ± 10.2	3.25 ± 0.54
Parmax/BP-4	16.7 ± 3.13	334.1 ± 13.1	2.46 ± 0.96
Parmax/BP-5	33.4 ± 2.54	387.3 ± 16.7	1.37 ± 0.32

Figure 13 shows the cross-sectional fracture of the Parmax/BP composites after tensile testing. This further verifies the dispersion quality and the reinforcing mechanism of the MWNTs. The well-dispersed lines seen in Figure 13 are the ends of the fractured MWNTs. This failure mechanism indicates adequate load transfer to the MWNTs as opposed polymer matrix failure and nanotube pull-out characteristics. Moreover the polymers still remain on the pull-out nanotubes after tensile testing, as shown in Figure 13(b). This kind of nanotube fracture upon tensile testing reflects a strong interfacial adhesion between the MWNTs and LCP matrix, allowing for adequate load transfer from the polymer matrix to the nanotubes.[39]

By adding a small amount of MWNTs (6.23 wt %) in the Parmax LCP resin, we can achieve a significant improvement in mechanical properties, compared to other cases where thermosetting and non-LCP thermoplastics, such as polycarbonate and polyamide, were used.[50] This is potentially due to a combination of several factors, including homogenous dispersion of MWNTs, strong interfacial adhesion due to π-stacking interaction,[45] and the alignment of MWNTs and LCP chains in the LCP matrix. The aligned packing of the MWNTs with the LCP matrix improved the load transfer due to enhancing the interfacial bonding between the LCP matrix and the MWNTs.

Electrical Conductivity

CNTs are an excellent candidate for use in conductive nanocomposites due to their high electrical conductivity and high aspect ratio. The dispersion and alignment of MWNTs in the polymer matrix is known to play an important role in

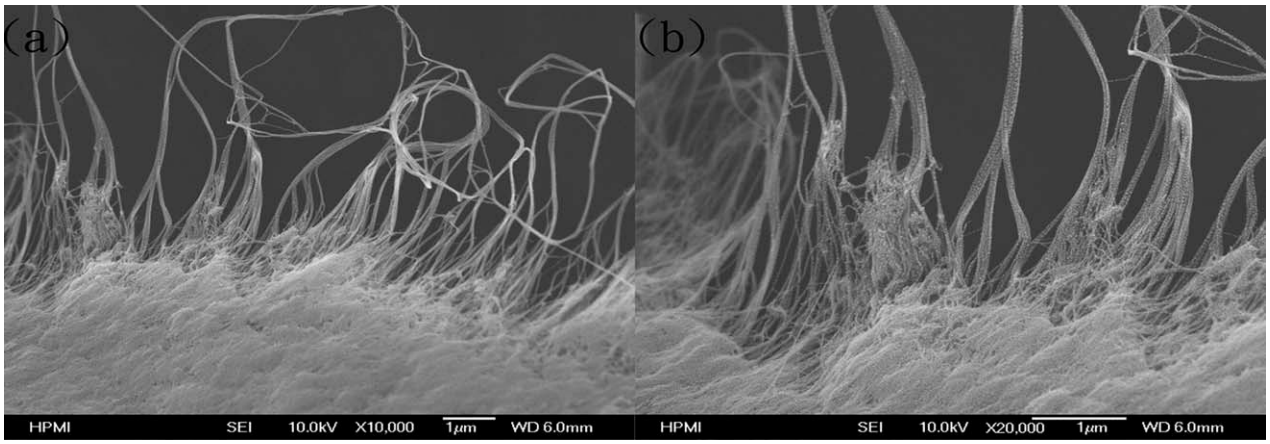

Figure 13. SEM morphology of the cross-sectional fracture surface of the Parmax/BP nanocomposite after tensile testing: (a) low magnification, (b) high magnification.

determining the electrical properties of the polymer composites directly. Compared to carbon black and conventional conductive carbon fibers, MWNTs can form the conductive pathway in polymer composites at a relatively low volume fraction as they possess very high aspect ratio, generally in the range of 100–1000.[51] Figure 14 shows the electrical conductivity of the Parmax/BP nanocomposites as a function of the MWNT concentration. Parmax is an insulator with an electrical conductivity of approximately 10^{-13} S/cm. As seen in Figure 14, the electrical conductivity of composite was dramatically enhanced by introduction of BP. When two layers of CNT sheets were added to the Parmax (Parmax/BP-2, 1.13 wt % MWNT), the conductivity increased to 13.14 S/cm, an enhancement of approximately 13 orders of magnitude compared to that of the neat Parmax. When five layers of CNT sheets were added (Parmax/BP-5, 6.23 wt % MWNT), the conductivity was enhanced to approximately 100.23 S/cm. The conductivity of the Parmax/BP-5 sample was significantly higher than that of composites containing low wt % CNT content by using regular mixing dispersion approach.[52] These high conductivity measurements may attribute to the MWNT alignment and the dense packing of MWNT BP, leading to better contact among the nanotubes.

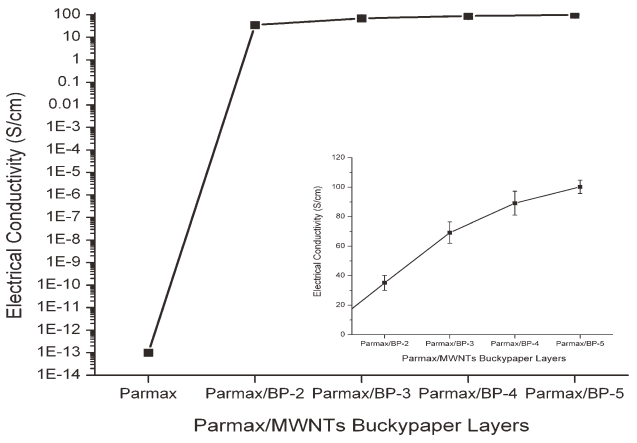

Figure 14. Effect of MWNT concentration on electrical conductivity of Parmax/BP nanocomposites compared to neat Parmax.

CONCLUSIONS

In this study, the Parmax/BP composites were prepared using layer-by-layer assembly and hot press method. The thermal, mechanical, and electrical properties of the resultant samples were characterized. The highly aromatic structure of Parmax contributed to more intense interactions between the polymer chains and the CNTs in the BP. SEM and X-ray characterizations revealed a highly dispersed and aligned network of MWNTs within the LCP matrix. The thermal properties of the composite increased significantly with the increasing MWNT concentration compared to the neat Parmax sample. The improvement in the composite mechanical properties compared to the neat polymer was primarily due to strong interfacial adhesion between the MWNTs and the LCP matrix, and the induced CNT and polymer chain alignment. With the addition of five layers of BP (6.23 wt % MWNT), the tensile strength and modulus of the nanocomposite improved by 110% and 750%, respectively. The incorporation of BP also produces a conductive network even at low nanotube concentration (1.13 wt % MWNT), leading to a high electrical conductivity of approximately 100.23 S/cm (Parmax/BP-5, 6.23 wt % MWNT) for potential multifunctional applications. The ongoing work is directed toward the further simulation and investigation of CNT aligning behavior in Parmax/BP composite and π-stacking interaction induced alignment as well.

ACKNOWLEDGMENTS

This research is supported by ONR (N00014-11-1-0274) project. The sponsorship and oversight of the program by Dr. Ignacio Perez are greatly appreciated.

REFERENCES

1. Dresselhaus, M. S.; Dresselhaus, G.; Eklund, P. C. In: Dresselhaus, M. S.; Dresselhaus, G.; Eklund, P. C. Science of Fullerenes and Carbon Nanotubes; Academic Press: San Diego, **1996;** p 292.
2. Salvetat, J. P.; Bonard, J. M.; Thomson, N. H.; Kulik, A. J.; Forró, L.; Benoit, W.; Zuppiroli, L. Appl. Phys. *A* **1999,** *69,* 255.

3. Treacy, M. M. J.; Ebbesen, T. W.; Gibson, J. M. *Nature* **1996,** *381*, 678.
4. Iijima, S. *Nature* **1991,** *354*, 56.
5. Liu, J.; Rinzler, A. G.; Dai, H.; Hafner, J. H.; Bradley, R. K.; Boul, P. J.; Lu, A.; Iverson, T.; Shelimov, K.; Huffman, C. B.; Rodriguez-Macias, F.; Shon, Y.-S.; Lee, T. R.; Colbert, D. T.; Smalley, R. E. *Science* **1998,** *280*, 1253.
6. Bae, D. J.; Kim, K. S.; Park, Y. S.; Suh, E. K.; An, K. H.; Moon, J.-M.; Lim, S. C.; Park, S. H.; Jeong, Y. H.; Lee, Y. H. Phys. Rev. *B* **2001,** *64*, 233401.
7. Knapp, W.; Schleussner, D.; Wüest, M. J. *Phys. Conf. Ser.* **2008,** *100*, 092007.
8. Cooper, S. M.; Chuang, H. F.; Cinke, M.; Cruden, B. A.; Meyyappan, M. *Nano Lett.* **2003,** *3*, 189.
9. Zhang, X.; Sreekumar, T. V.; Liu, T.; Kumar, S. J. Phys. Chem. *B* **2004,** *108*, 16435.
10. Baughman, R. H.; Cui, C.; Zakhidov, A. A.; Iqbal, Z.; Barisci, J. N.; Spinks, G. M.; Wallace, G. G.; Mazzoldi, A.; De Rossi, D.; Rinzler, A. G.; Jaschinski, O.; Roth, S.; Kertesz, M. *Science* **1999,** *284*, 1340.
11. Vohrer, U.; Kolaric, I.; Haque, M. H.; Roth, S.; Detlaff-Weglikowska, U. *Carbon* **2004,** *42*, 1159.
12. Prasad, D.; Zhiling, L.; Satish, N.; Barrera, E. V. *Nanotechnology* **2004,** *15*, 379.
13. Li, F.; Cheng, H. M.; Bai, S.; Su, G.; Dresselhaus, M. S. *Appl. Phys. Lett.* **2000,** *77*, 3161.
14. Zhang, C.-S.; Ni, Q.-Q.; Fu, S.-Y.; Kurashiki, K. *Compos. Sci. Technol.* **2007,** *67*, 2973.
15. Thostenson, E. T.; Chou, T.-W. *Carbon* **2006,** *44*, 3022.
16. Odom, T.; Hafnerand, J.; Lieber, C.; Dresselhaus, M.; Dresselhaus, G.; Avouris, P., Eds. Scanning probe microscopy studies of carbon nanotubes. Springer: Berlin/Heidelberg, **2001; p 173.**
17. Ma, P.-C.; Siddiqui, N. A.; Marom, G.; Kim, J.-K. *Composites A* **2010,** *41*, 1345.
18. Hu, X.; Kobatake, H. *Acoust. Sci. Technol.* **2003,** *24*, 53.
19. Ismach, A.; Joselevich, E. *Nano Lett.* **2006,** *6*, 1706.
20. Bin, Y.; Kitanaka, M.; Zhu, D.; Matsuo, M. *Macromolecules* **2003,** *36*, 6213.
21. Xin, H.; Woolley, A. T. *Nano Lett.* **2004,** *4*, 1481.
22. Krupke, R.; Hennrich, F.; Löhneysen, H. v.; Kappes, M. M. *Science* **2003,** *301*, 344.
23. Collings, P. J.; Hird, M. Introduction To Liquid Crystals Chemistry And Physics; Taylor & Francis: London, UK **1997.**
24. Geary, J. M.; Goodby, J. W.; Kmetz, A. R.; Patel, J. S. *J. Appl. Phys.* **1987,** *62*, 4100.
25. Hongladarom, K.; Burghardt, W. R.; Baek, S. G.; Cementwala, S.; Magda, J. J. *Macromolecules* **1993,** *26*, 772.
26. Hamley, I. W.; Davidson, P.; Gleeson, A. J. *Polymer* **1999,** *40*, 3599.
27. Song, W.; Kinloch, I. A.; Windle, A. H. *Science* **2003,** *302*, 1363.
28. Lynch, M. D.; Patrick, D. L. *Nano Lett.* **2002,** *2*, 1197.
29. Mrozek, R. A.; Kim, B.-S.; Holmberg, V. C.; Taton, T. A. *Nano Lett.* **2003,** *3*, 1665.
30. Cheng, Q.; Wang, B.; Zhang, C.; Liang, Z. *Small* **2010,** *6*, 763.
31. Vuorinen, A.-M.; Dyer, S. R.; Lassila, L. V. J.; Vallittu, P. K. Compos. *Interfaces* **2011,** *18*, 387.
32. Sreekumar, T. V.; Liu, T.; Kumar, S.; Ericson, L. M.; Hauge, R. H.; Smalley, R. E. *Chem. Mater.* **2002,** *15*, 175.
33. Islam, M. F.; Rojas, E.; Bergey, D. M.; Johnson, A. T.; Yodh, A. G. *Nano Lett.* **2003,** *3*, 269.
34. Paredes, J. I.; Burghard, M. *Langmuir* **2004,** *20*, 5149.
35. Ying, T.; Jin Gyu, P.; Qunfeng, C.; Zhiyong, L.; Chuck, Z.; Ben, W. *Nanotechnology* **2009,** *20*, 335601.
36. Shim, B. S.; Tang, Z.; Morabito, M. P.; Agarwal, A.; Hong, H.; Kotov, N. A. *Chem Mater* **2007,** *19*, 5467.
37. Koerner, H.; Liu, W.; Alexander, M.; Mirau, P.; Dowty, H.; Vaia, R. A. *Polymer* **2005,** *46*, 4405.
38. Sahoo, N. G.; Cheng, H. K. F.; Li, L.; Chan, S. H.; Judeh, Z.; Zhao, J. *Adv. Funct. Mater.* **2009,** *19*, 3962.
39. X.-L.Xie, Mai, Y.-W.; Zhou, X.-P. *Mater Sci Eng R: Rep* **2005,** *49*, 89.
40. Dijkstra, D.; Karbach, A.; Malkovich, N. *J. Mater. Sci.* **2007,** *42*, 3810.
41. Ge, J. J.; Hou, H.; Li, Q.; Graham, M. J.; Greiner, A.; Reneker, D. H.; Harris, F. W.; Cheng, S. Z. D. *J. Am. Chem. Soc.* **2004,** *126*, 15754.
42. Jin, L.; Bower, C.; Zhou, O. *Appl. Phys. Lett.* **1998,** *73*, 1197.
43. Díez-Pascual, A. M.; Naffakh, M.; Gómez, M. A.; Marco, C.; Ellis, G.; Martínez, M. T.; Ansón, A.; González-Domínguez, J. M.; Martínez-Rubi, Y.; Simard, B. *Carbon* **2009,** *47*, 3079.
44. Jaćović, M. S.; Pollock, D.; Porter, R. S. *J. Appl. Polym. Sci.* **1979,** *23*, 517.
45. Wu, Q.; Bao, J.; Zhang, C.; Liang, R.; Wang, B. *J. Therm. Anal. Calorim.* **2011,** *103*, 237.
46. Moniruzzaman, M.; Winey, K. I. *Macromolecules* **2006,** *39*, 5194.
47. Biswas, S.; Fukushima, H.; Drzal, L. T. *Composites A* **2011,** *42*, 371.
48. Endo, M.; Takeuchi, K.; Hiraoka, T.; Furuta, T.; Kasai, T.; Sun, X.; Kiang, C. H.; Dresselhaus, M. S. J. Phys. Chem. *Solids* **1997,** *58*, 1707.
49. Shen, J.; Huang, W.; Wu, L.; Hu, Y.; Ye, M. *Compos. Sci. Technol.* **2007,** *67*, 3041.
50. Spitalsky, Z.; Tasis, D.; Papagelis, K.; Galiotis, C. *Prog. Polym. Sci.* **2010,** *35*, 357.
51. Shaffer, M. S. P.; Windle, A. H. *Adv. Mater.* **1999,** *11*, 937.
52. Mukherjee, M.; Das, T.; Rajasekar, R.; Bose, S.; Kumar, S.; Das, C. K. *Composites A* **2009,** *40*, 1291.